Applied Catalysis B: Environmental 291 (2021) 120038

Contents lists available at ScienceDirect

Applied Catalysis B: Environmental

journal homepage: www.elsevier.com/locate/apcatb

Effects of solar irradiation on thermally driven CO_2 methanation using Ni/CeO_2–based catalyst

Viktoria Golovanova [a,*], Maria Chiara Spadaro [b], Jordi Arbiol [b,c], Viacheslav Golovanov [d], Tapio T. Rantala [e], Teresa Andreu [a], Joan Ramón Morante [a,f]

[a] Catalonia Institute for Energy Research (IREC), Jardins de les Dones de Negre 1, 08930, Sant Adrià de Besòs, Spain
[b] Catalan Institute of Nanoscience and Nanotechnology (ICN2), CSIC and BIST, Campus UAB, Bellaterra, Barcelona, Catalonia, 08193, Spain
[c] ICREA, Pg. Lluís Companys 23, 08010, Barcelona, Catalonia, Spain
[d] South–Ukrainian National University, Staroportofrankovskaya str. 26, 65020, Odessa, Ukraine
[e] Department of Physics, Tampere University, P.O. Box 692, FI-33014, Tampere, Finland
[f] Department of Electronics, University of Barcelona (UB), Marti i Franquès 1, 08028, Barcelona, Spain

ARTICLE INFO

Keywords:
CO_2 methanation
LSPR
Photothermal effect
Nickel-ceria catalyst
DRIFTS

ABSTRACT

Utilization of the renewable energy sources is one of the main challenges in the state-of-the-art technologies for CO_2 recycling. Here we have taken advantage of the solar light harvesting in the thermocatalytic approach to carbon dioxide methanation. The large-surface-area Ni/CeO_2 catalyst produced by a scalable low-cost method was characterized and tested in the dark and under solar light irradiation conditions. Light-assisted CO_2 conversion experiments as well as in-situ DRIFT spectrometry, performed at different illumination intensities, have revealed a dual effect of the incident photons on the catalytic properties of the two-component Ni/CeO_2 catalyst. On the one hand, absorbed photons induce a localized surface plasmon resonance in the Ni nanoparticles followed by dissipation of the heat to the oxide matrix. On the other hand, the illumination activates the photocatalytic properties of the CeO_2 support, which leads to an increase in the concentration of the intermediates being precursor for methane production. Analysis of the methane production at different temperatures and illumination conditions has shown that the methanation reaction in our case is controlled by a photothermally-activated process. The used approach has allowed us to increase the reaction rate up to 2.4 times and consequently to decrease the power consumption by 20 % under solar illumination, thus replacing the conventional thermal activation of the reaction with a green energy source.

1. Introduction

Conversion of carbon dioxide to renewable hydrocarbon fuels, such as methane, is a big challenge nowadays due to the high thermodynamic stability of the CO_2 molecule and, therefore, major difficulties in its reduction [1–3]. The standard thermocatalytic approach for CO_2 methanation requires relatively high temperatures (150−500 °C) [4], which gives rise to a number of alternative approaches to replace or assist thermochemical catalysis [5–8]. Plasma-assisted methanation of CO_2 was reported, being efficient even at room temperature [9,10] with promising performances. Another important field of research is related to the utilization of solar light as an additional green energy source for CO_2 hydrogenation to methane [11–15]. Except for the standard photocatalytic approach, based on the metal-decorated metal oxides, where the metal oxide support is used as the main photoabsorber and metallic nanoparticles act only as active catalytic sites [16,17], a rapidly emerging field in catalysis is taking advantage of the strong light extinction of the metallic nanoparticles themselves, owning to the effect called localized surface plasmon resonance (LSPR) [18,19]. The LSPR-driven catalysis is mostly making use of noble metals (Au and Ag) due to their strong plasmonic response in the visible and UV part of the spectrum [20–24]. However, other abundant and non-expensive metals, in particular some of the VIII group transition metals, such as Ni have also proven to exhibit plasmonic features [11,25–29], although less pronounced due to the higher damping. Moreover, nickel nanoparticles in combination with metal oxides presenting high oxygen mobility, such as CeO_2, have been proposed as a candidate catalyst for the efficient thermal conversion of CO_2 to methane [30].

* Corresponding author.
E-mail address: vholovanova@irec.cat (V. Golovanova).

https://doi.org/10.1016/j.apcatb.2021.120038
Received 26 November 2020; Received in revised form 3 February 2021; Accepted 15 February 2021
Available online 23 February 2021
0926-3373/© 2021 The Authors. Published by Elsevier B.V. This is an open access article under the CC BY license (http://creativecommons.org/licenses/by/4.0/).

Excited LSPR is followed by a strong near-field enhancement, which is then damped through one of the possible mechanisms: i) radiative decay through re-emitting of the photons; ii) Landau damping, resulting in a non-equilibrium charge distribution (so-called "hot electrons" or "hot holes", which then can be transferred to the metal-oxide support or directly participate in the catalytic reaction); or iii) direct excitation of electron-hole pairs in the semiconductor through plasmon-induced resonant energy transfer (PIRET). Another effect that has been recently introduced, consists in direct metal-to-semiconductor charge transfer [31,32]. All of the damping mechanisms stated above occur in the timescale of 1–100 fs and, eventually, lead to recombination of the created non-equilibrium charge carriers (0.1–100 ps) and result in strong local heating (0.1–10 ns) [33]. The plasmon damping has found a lot of applications, and many works are dedicated to exploiting of the "direct" improvement of catalytic properties by plasmonic hot electrons [20,25,34–37].

However, few works have emphasized the importance of the catalytic performance enhancement of the Ni-based catalysts due to plasmon-induced self-heating of nickel nanoparticles followed by a dissipation of heat to the oxide matrix. Due to the excellent photothermal properties of Ni nanoparticles [26,38–40], this effect in many cases can be considered as the main consequence of the plasmon excitation in Ni-based catalysts as compared with direct hot electrons interface transfer. In this work, we have used a wet impregnation of mesoporous silica SBA-15 template to prepare a high surface area Ni/CeO_2 catalyst for CO_2 methanation where a large size distribution of Ni nanoparticles allows us to perform highly selective and energetically efficient methanation of CO_2 assisted by plasmonic heating of the catalysts with solar light. The use of in-situ characterization has revealed the mechanism of CO_2 hydrogenation and the optimal conditions for the plasmon-assisted methanation reaction, which allows us to increase the productivity up to 2.4 times and reduce the energy consumption by 20 % as compared to the conventional thermochemical approach. Furthermore, we have corroborated that under solar illumination conditions, in spite of the significant increase of the formate intermediates due to the photocatalytic properties of CeO_2, the rate of methane production is limited by the thermally-controlled step, related to formate hydrogenation reactions. A complete understanding of these phenomena is fundamental for the new design of efficient plasmonic NP-semiconductor-based catalysts for thermally driven methanation reactors.

2. Experimental

2.1. Catalyst synthesis

SBA-15 mesoporous silica templates were synthesized by the following process, based on the one described in [41]: 9 g of Pluronic® P123 (polyethylene glycol-*block*-polypropylene glycol-*block*-polyethylene glycol, average M_n ~5,800, Sigma-Aldrich) was mixed with 90 g of diluted HCl (50 wt.%) and 245 g of Milli-Q water and stirred at 38 °C to obtain polymeric micelles. 18.7 g of TEOS (tetraethyl orthosilicate, 98 %, Sigma-Aldrich) was added as a silica precursor. The reaction was held for another 24 h at 100 °C, after which the mixture was filtered and eventually calcined at 550 °C for 5 h.

The Ni/CeO_2 catalyst was prepared by simultaneous impregnation of SBA-15 templates (1.05 g) with 6.5 mL of 0.6 M cerium (III) nitrate hexahydrate (Sigma-Aldrich) and 3 mL of 0.6 M nickel (II) nitrate hexahydrate (Sigma-Aldrich). The Ni/Ce ratio was chosen in such a way that the estimated Ni weight concentration in the final product would be 15 %. The reaction was held in two steps, to achieve a high degree of impregnation [41,42]: first with impregnation of the solutions to the mesoporous silica and annealing at 350 °C for the preliminary precursor decomposition, and second impregnation with half of the initial amounts, followed by annealing of the sample at 800 °C. The silica template was further dissolved in 2 M NaOH for 12 h at 70 °C with constant stirring. The obtained NiO/CeO_2 powder was further reduced in hydrogen atmosphere (5% H_2 and 95 % Ar) for 7 h at 450 °C to get the Ni/CeO_2 catalyst (Scheme 1).

For comparison, samples without Ni were also prepared using the same template impregnation technique. 6.5 mL of 0.6 M cerium nitrate hexahydrate was added to 0.9 g of SBA-15, and the same two-step procedure was applied for calcination and second impregnation of silica template.

2.2. Physico-chemical characterization

XRD spectra were recorded on a Bruker type XRD D8 diffractometer (CuKα radiation, λ = 1.5418 Å, 40 kV, 40 mA) with a scanning range of 2Θ from 20° to 80° and step size of 0.05°/3 s. The average crystalline sizes of metallic nanoparticles were derived from the Scherrer's equation $D = \frac{K\lambda}{\beta\cos\theta}$, where Θ is the Bragg angle, K is the shape factor, λ is the X-ray wavelength and β is the full width of the diffraction peak at half maximum (FWHM).

Scanning electron microscope (SEM, Zeiss Auriga 60) was used to study the morphology of the samples. The composition of the synthetized catalyst was studied by energy dispersive X-ray spectroscopy (EDX, Oxford Inca Energy).

N_2-physisorbtion analysis was conducted in TriStar II 3020-Micrometrics equipment at liquid nitrogen temperature. Before the measurements, the samples were degassed under vacuum conditions at 90 °C for 1 h and then at 250 °C for 3 h. Brunauer-Emmett-Teller (BET) method was applied for calculation of the BET surface area for a relative pressure (P/P_0) range of 0.1−0.3. The total pore volume and the average pore size were determined by applying Barrett-Joyner-Halenda (BJH) method to desorption branch of the isotherms at the value $P/P_0 = 0.95$.

H_2-TPR (hydrogen temperature programmed reduction) and CO-chemisorption were carried out using an automated chemisorption analyzer (Autochem HP-Micrometrics). In case of H_2-TPR measurements 100 mg of powder sample was kept under constant 5% H_2/Ar flow, while the temperature was increased from 25 °C to 800 °C with a heating ramp of 10 °C/min. The consumed H_2 was measured using a thermal conductivity detector (TCD). The CO-chemisorption measurements were held at 35 °C under the flow of 10 %CO/He over the samples, which were pre-reduced at 450 °C under 5% H_2/Ar flow for 7 h. Pulses of CO were periodically introduced until full saturation of the system. Active metal surface area and metal dispersion were calculated assuming the stoichiometric ratio CO/Ni equal to 1, Ni atomic weight to 58.71, its atomic cross-sectional area to 0.0649 nm^2 and density to 8.9 g/cm^{-3}.

UV–vis light absorption spectra were measured using the Perkin Elmer Lambda 35 UV–vis spectrometer in the diffuse reflectance mode. Absorption of the samples was calculated according to the equation: $A = 1 - R$, as no transmission was observed.

High-resolution transmission electron microscopy (HRTEM) together with scanning TEM (STEM) investigation was performed on a field emission gun FEI Tecnai F20 microscope. High angle annular dark-field (HAADF) STEM was combined with electron energy loss spectroscopy (EELS) in the Tecnai microscope by using a GATAN QUANTUM filter.

2.3. Functional characterization

A custom-made flow-type gas reactor (Scheme S1(b)) was created in order to allow simultaneous heating and illumination of the catalyst. 50 mg of the catalyst were spread uniformly over an aluminum support, whereas its temperature was constantly measured by a K-type thermocouple. An intimate contact was preserved throughout the reaction in order to measure directly the changes in the catalyst temperature.

The catalyst was preliminarily reduced in hydrogen atmosphere (5% H_2 and 95 % Ar) for 7 h at 450 °C. The methanation reaction was held under a constant flow of 80 % H_2 and 20 % CO_2 gas mixture (99.999 %,

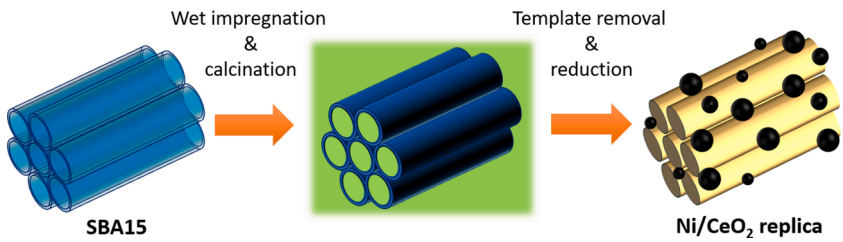

Scheme 1. Ni/CeO_2 catalyst fabrication process.

Linde) at a rate of 20 mL min^{-1}. The outlet gas flow passed through a cold liquid-gas separator (5 °C) for water condensation, and was measured by a mass flow meter (MF, Bronkhorst). The gas products (CH_4, CO, CO_2 and H_2) were analyzed using a 490 microGC gas chromatograph (Agilent Technologies).

The methane yield was calculated according to the equation:

$$Y_{CH_4}(\%) = \frac{X_{CO_2}(\%) \times S_{CH_4}(\%)}{100\%},$$

where $X_{CO_2}(\%) = \frac{\Phi_{CO_2,in} - \Phi_{CO_2,out}}{\Phi_{CO_2,in}}$ is the conversion of CO_2 and $S_{CH_4}(\%) = \frac{\Phi_{CH_4,out}}{\Phi_{CO_2,in} - \Phi_{CO_2,out}}$ is the selectivity to methane. $\Phi_{CO_2,in}, \Phi_{CO_2,out}$ are the CO_2 molar flows in the inlet and in the outlet, respectively, and $\Phi_{CH_4,out}$ is the CH_4 molar flow in the outlet. The catalytic activity was then evaluated from the following equation:

$$k = \frac{\Phi}{m} \times \frac{Y_{CH_4}(\%)}{100\%}$$

The reported data were the average values, taken from five measurements for each temperature point, with the measurement error less than 3%. Carbon mass balance was closed within the accuracy of ± 7%.

As a source of illumination, we used a 300 W solar simulator (Xe lamp, AM1.5 G filter) with a variable illumination power. The power density was measured by a laser powermeter (Gentec-EO UNO) containing a calibrated reference silicon cell. Bandpass filters (FGL400S, FGS900S, ThorLabs) were introduced to the system to cut a part of the spectrum as shown in Scheme S1(b).

Provided that methanation is an exothermic reaction, the temperature was allowed to reach a stable value in all of the studied conditions before any illumination was introduced.

2.4. In-situ DRIFTS characterization

In-situ diffuse reflectance infrared Fourier transform spectroscopy (DRIFTS) was used in order to study the nature of intermediate species formed during the methanation reaction over the Ni/CeO_2 catalyst under dark and light-assisted reaction conditions. The spectra were recorded using Bruker-Vertex70 spectrophotometer equipped with a high-temperature reaction control cell with two ZnSe windows, one quartz window and a catalytic bed. The catalyst was pre-reduced at 450 °C under 5% H_2/He flow of 50 mL/min for 1 h, then purged in He gas for 40 min to remove the residual H_2 from the cell and finally cooled down to desired temperature. The background spectrum was recorded in He at room temperature. CO_2 methanation reaction was performed in 20 mL/min of gas mixture (75 % of stoichiometric H_2/CO_2 ratio = 4 and 25 % of He balance) at 100 °C, 150 °C, 200 °C, 225 °C and 250 °C. Each measurement was recorded after 30 min in isothermal conditions, and followed by purging in He for 30 min to remove the excess water molecules. Spectra were recorded from 4200 cm^{-1} to 1000 cm^{-1} with a step of 1 cm^{-1}. Thermal analyzer Thermostat was used to control the product stream by their molecular weights (*m/z* ratios). The illumination (5 suns) during the DRIFTS measurement was applied through the quartz window from the solar simulator used during the functional characterization.

3. Results and discussion

3.1. Physical characterization of the catalyst

SEM and TEM images (Fig. 1) show that the obtained catalyst consists of CeO_2 nanofibers support (with a diameter of ~10 nm) and well-distributed Ni nanoclusters with the size distribution approximately from 5 to 50 nm. The EDX analysis shows the presence of 12 %(w.t.) Ni, which is in a good proximity with the initial estimations. Some residual silicon was spotted, which supposedly comes from the non-dissolved SBA-15 template, but its amount was as low as 1% of the catalyst mass.

The ceria support, shown in Fig. 1(d), has a typical channel shape due to the SBA-15 template where each channel is 8 nm distant to the closest. This configuration of the support leads to its mesoporous properties and allows the small Ni clusters to penetrate inside the ceria structure.

HRTEM study has shown that the used synthesis procedure is suitable to create a ceria-supported catalyst with a presence of highly distributed small Ni nanoparticles (~5 nm) which have a strong interaction with the ceria support (Fig. 2). They are mostly located in the voids between the ceria rods. CO_2 methanation over Ni/CeO_2 is a complex reaction, requiring simultaneous H_2 and CO_2 activation. The former occurs on the metallic Ni sites and the latter on the basic sites of CeO_2 [43]. The challenge of the catalyst design is that products of these two reaction steps (H* and CO_x) are separated by a spatial constraint, which has to be minimized in order to achieve better catalytic performance. From this point of view, highly distributed Ni nanoclusters embedded in the mesoporous CeO_2 (Fig. 1(d)) represent the optimal catalyst configuration for CO_2 methanation. We assume that the high exposure of the boundary phase Ni/CeO_2 to the gas is responsible for the significant CO_2 conversion.

From the low-magnification images (Figs. 1(d); S1(a), Ni panel) we can also see the presence of bigger Ni clusters (~20–50 nm). They are located mostly on the surface of the catalyst and therefore play the major role in the solar light absorption and scattering. Relatively high distribution of the nanoclusters' sizes is responsible for broadening of the plasmonic extinction peak and black coloring of the reduced powder.

The N_2-physisorption analysis of the silica SBA-15 template, CeO_2 and Ni/CeO_2 replica has shown that the obtained powders possess a mesoporous structure with a high BET surface area. The surface areas and pore dimensions of pure CeO_2 support and Ni/CeO_2 catalyst used in this study are quite similar, which indicates that Ni impregnation has not influenced the mesoporous morphology of the ceria support. Moreover, the Ni/CeO_2 catalyst exhibits a good dispersion of Ni nanoparticles with high metal surface area, which was derived from CO-chemisorption analysis (Table 1).

H_2-TPR analysis was used to study reduction properties of the obtained catalyst (Fig. 3). The Ni/CeO_2 sample presents a strong peak at T =328 °C and two smaller ones at T =213 °C and T =271 °C, attributed to the reduction of the weakly bound NiO species on the CeO_2 surface [44]. The more intensive one is related to the reduction of smaller nanoparticles, whereas the low-temperature peaks are due to the large NiO particles on the CeO_2 support. The peak at T =442 °C was assigned to the reduction of strongly bound NiO [45], and the high-temperature process

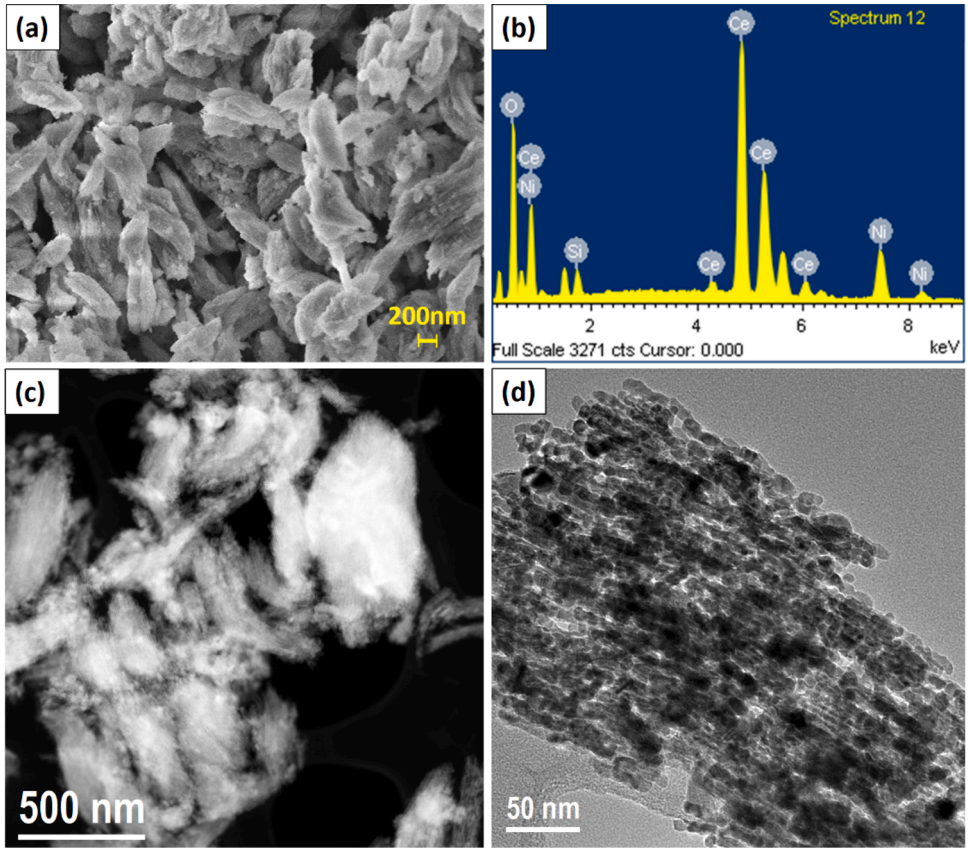

Fig. 1. SEM image of the Ni/CeO_2 catalyst (a) and the corresponding EDX spectrum (b); HAADF STEM (c) and TEM (d) general view images of the sample at low magnification.

at T =697 °C was attributed to the Ce^{4+} to Ce^{3+} reduction in CeO_2 [46].

The H_2-TPR analysis confirmed that the reduction temperature of 450 °C (dashed line on Fig. 3), chosen for NiO/CeO_2 catalyst is sufficient to reduce all the types of NiO clusters. EELS chemical composition maps prove that the Ni present in the reduced sample is mostly metallic (Fig. S1).

Fig. 4 shows XRD spectra of the as-prepared samples and reduced under H_2 atmosphere (5% H_2 in Ar, 7 h, 450 °C). As we can see from the figure, NiO phase, that was present in the as-prepared catalyst, disappears completely in favor of metallic Ni. The peaks attributed to CeO_2 are shifted with respect to the clear CeO_2 phase in case of the non-reduced samples, which indicates the incorporation of Ni atoms and nanoclusters to CeO_2, causing stress onto the lattice [47]. This shift can be clearly seen on the inset of Fig. 4, where the CeO_2 diffraction peak (56.34°) present in both pure CeO_2 and reduced Ni/CeO_2 samples, is shifted to 56.41° in the case of non-reduced NiO/CeO_2. After reducing, all Ni is removed from the CeO_2 lattice, which results in shifting of the peaks back to the positions of the CeO_2 phase. It is also worth noticing, that the peak is broadened with respect to the pure CeO_2 support, which indicates the stress and the lattice parameter inhomogeneity due to the presence of the Ni atoms and nanoclusters inside of the CeO_2 rods. The crystallite sizes of Ni particles were estimated by Sherrer's equation using the peak of $2\Theta = 44.51°$. The average size was found to be 27.9 nm, which is in accordance with the nanoparticle dimensions extracted from the TEM data.

In order to analyze the possible strain influence of the Ni nanoparticles embedded in the CeO_2 mesoporous channels, we used the Geometrical Phase Analysis (GPA) routines in the Digital Micrograph software [48]. Our GPA analyses showed a relative compression of the CeO_2 lattice planes when they are close to a Ni nanoparticle (Fig. S2). The profile obtained along the dark blue arrow pointed out in the figure corroborates that the CeO2 {111} planes suffer a 4–5 % compression close to the Ni nanoparticle, which is in line with the previous XRD analysis.

3.2. *Catalytic performance of the catalyst in the CO_2 methanation reaction*

We performed functional characterization of the synthetized catalyst in the tubular-type reactor in dark conditions (Scheme S1(a)). The measured catalytic activity at different reaction temperatures is shown on the Fig. 5(a). We found that CO_2 conversion reaches 80 % at 300 °C, and the selectivity to methane was as high as 95 %.

Due to its high surface area the catalytic activity of Ni/CeO_2 catalyst used in this work is comparable to the activity of the other Ni/CeO_2 catalysts reported previously [49,50].

We have also carried out a stability test which has revealed a high stability of the catalyst under constant reaction conditions at T =270 °C (Fig. 5(b)).

3.3. *Photothermal effects*

UV–vis spectroscopy was used to measure the reflectance of bare CeO_2 and Ni/CeO_2 samples. The obtained data were transformed into absorption as no transmittance was observed. As it can be seen from the Fig. 6(a), bare cerium oxide powder does not absorb under IR and visible illumination, but starts absorbing strongly starting from 430 nm, which corresponds to the reported band gap of oxygen vacancy-enriched CeO_2 nanoparticles (2.87 eV) [51]. In contrast, samples with Ni nanoparticles exhibit an extraordinary high absorption over all of the measured illumination range. We attribute this significant rise in the visible and IR light absorption to the localized surface plasmon resonance of the Ni

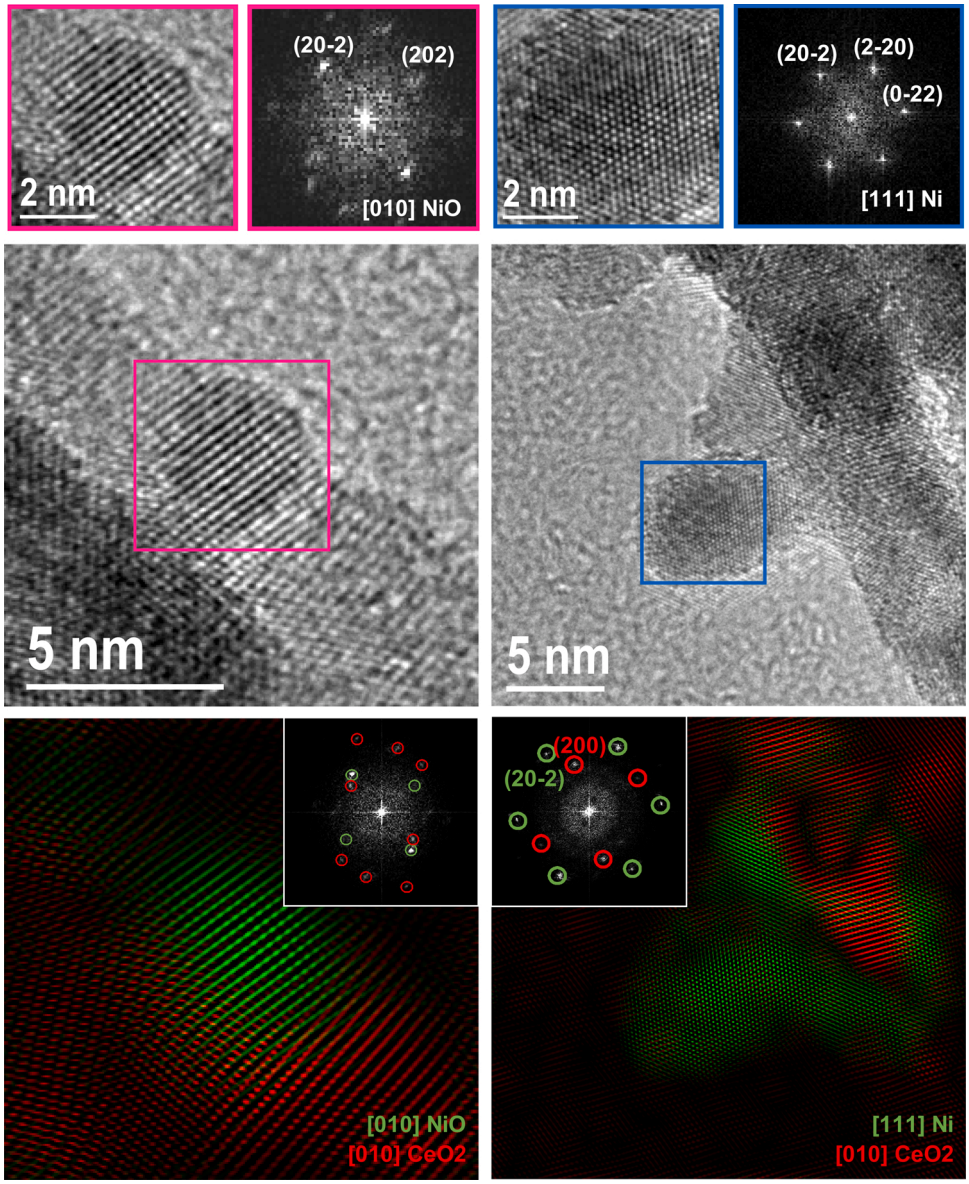

Fig. 2. HRTEM micrographs of a detail of the non-reduced NiO/CeO_2 (left) and reduced Ni/CeO_2 (right) nanostructures. In the top panel we report the magnification in the squared area and the corresponding indexed power spectra. In the bottom panel, we report the frequency filtered maps evidencing NiO, Ni and CeO_2 planes with different colors.

Table 1
N_2-physisorption and CO-chemisorption analysis data of the Ni/CeO_2 catalyst, pure CeO_2 support and SBA-15 mesoporous silica template.

Sample	Surface area, m^2/g	Micropore volume, cm^3/g	Pore size, nm	Ni dispersion, %	Active metal surface area, m^2/g_{Ni}
SBA-15	866.2	0.99	6.6	–	–
CeO_2	121.1	0.21	3.3	–	–
Ni/ CeO_2	103.5	0.20	2.9	1.3	8.6

nanoparticles, which is known to have a broad band in the IR-vis range, as was previously reported [52–54].

To take advantage of the extra light absorption of the catalyst used in this work, we performed a series of CO_2 methanation tests under solar illumination. We observed a significant increase in the CH_4 yield under illumination, which was concomitant with a temperature increase in the reactor.

Although the plasmonic Ni nanoparticles have a higher damping factor comparing to frequently used Au or Ag nanoparticles, the overlap of their absorption spectrum with the solar one is much better [55]. This ensures an effective absorption of the solar illumination and transforming it to heat.

We have used three different light intensities and operated at three different starting temperatures in order to study the effects related to the photoinduced catalytic activity. Also, in order to investigate the nature of the activity enhancement, we performed wavelength-dependent tests by introducing bandpass filters into the experimental setup. UV filter ($\lambda > 400$ nm) was used to cut off the UV part of the solar spectrum, while the IR filter ($\lambda < 800$ nm) removed the near-IR and IR photons. Transmission spectra of the used filters are shown on the Fig. 6(b). We have used the combination of two bandpass filters in order to study the pure effect of visible light on the CO_2 conversion. It is worth noting that introducing of the UV filter solely does not affect the catalytic performance of the Ni/CeO_2 catalyst, indicating that the absorption of light by CeO_2 is not responsible for the increase in the catalytic activity.

Fig. 7(a) sums up the changes in catalytic activity that occur in the

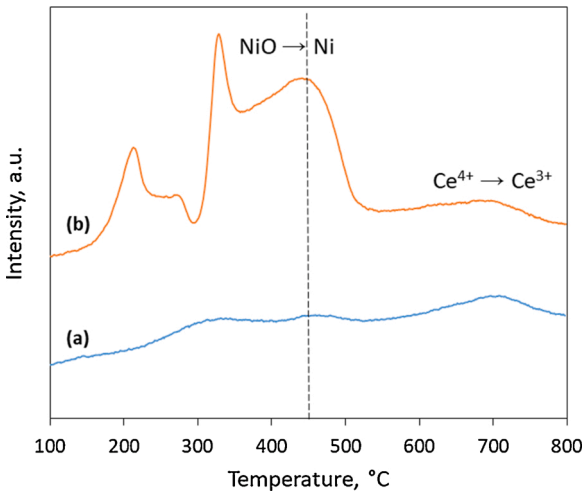

Fig. 3. H_2-TPR profile of the CeO_2 support (a) and Ni/CeO_2 catalyst (b).

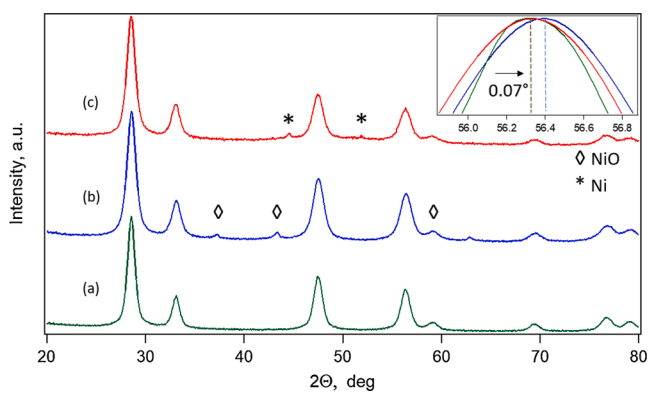

Fig. 4. XRD spectra of the CeO_2 support (a), non-reduced (b) and reduced (c) Ni/CeO_2 catalyst. The inset shows the shift of the 56.335 °CeO_2 diffraction peak in the non-reduced Ni/CeO_2 catalyst with respect to the reduced one and the pure CeO_2 support.

catalyst under solar light illumination at different temperatures, light intensities and illumination ranges. As it can be seen from the graph, introducing of visible light has a notable effect on the reaction rate, while the full solar spectrum induces an even higher increase to the catalytic activity. As it was stated previously, cutting off the UV part of the solar spectrum ($h\nu > 3.1$ eV) does not affect the reaction rate, thus neglecting the role of band-band electron transitions in ceria in the methane production enhancement. Eventually, the illumination of the catalyst may increase the rate of the methanation reaction as high as 2.4 times under suitable reaction conditions (Fig. 7(b)).

3.4. DRIFTS characterization

To study the effect of illumination on the intermediate steps of the reaction, we have performed in-situ DRIFTS experiments at different starting temperatures. The measurements were held both in dark conditions and under solar illumination. The corresponding spectra are shown on the Fig. 8 except the band at 2350 cm^{-1} corresponding to gas phase CO_2.

The pure CeO_2 samples without Ni nanoclusters show presence of hydroxyl groups with vibrations υ(OH) identified at 3725-3560 cm^{-1} and carbonate species only (Fig. S3). At 100 °C the surface is covered by bidentate carbonates (1586, 1300 cm^{-1}), bridged carbonates (1646, 1120 cm^{-1}) and hydrogen carbonates (1681, 1630, 1422, 1392 and 1212 cm^{-1}), presumably formed over OH groups on the CeO_2 surface. The temperature increase stimulates transformation of these carbonates into more stable mono- and polydentate carbonates (1483–1500, 1357 and 1150 cm^{-1}). In the absence of Ni° the dissociation of the H_2 molecule is not favored, and, therefore, formates are not formed on pure CeO_2 surface.

For Ni/CeO_2 catalyst at 100 °C no methane is produced, and CO_2 is mainly adsorbed on the basic Ce^{3+} sites [56,57], forming carbonate and hydrogen carbonates species, which are known as precursor for creation of formates. The bands at 1680 cm^{-1}, 1417 cm^{-1} and 1209 cm^{-1} were attributed to hydrogen carbonates vibrations, and the peak at 1642 cm^{-1} was assigned to bridged carbonates. The broad band (1472−1530 cm^{-1}) and a peak at 1150 cm^{-1} were attributed to mono- and polydentate carbonates. At 150 °C the weakly bound bridged carbonates are being transformed into mono- and polydentate carbonates and a new bands (1583, 1371 and 1343 cm^{-1}) attributed to formates begin to grow [58]. Starting from 200 °C a band attributed to production of methane appears at 3016 cm^{-1}. It grows further with the temperature increase, while the intensity of the formate peaks is being diminished. On the other hand, the band, attributed to mono- and polydentate carbonates, continuously grows with the temperature increase. This testifies that formates are the precursor in the methane formation, while the mono- and polydentate carbonates species do not take significant part in the reaction.

Under illumination, the DRIFTS spectra undergo some qualitative changes. At 100 °C the peaks at 1583 and 1371 cm^{-1}, attributed to vibration of monodentate formate (υ_{asym}(COO)) become much more pronounced, while the peaks related to hydrogen carbonate species (1680, 1417 or 1209 cm^{-1}) are distinctly decreased.

Another significant feature of the DRIFTS spectra, recorded under

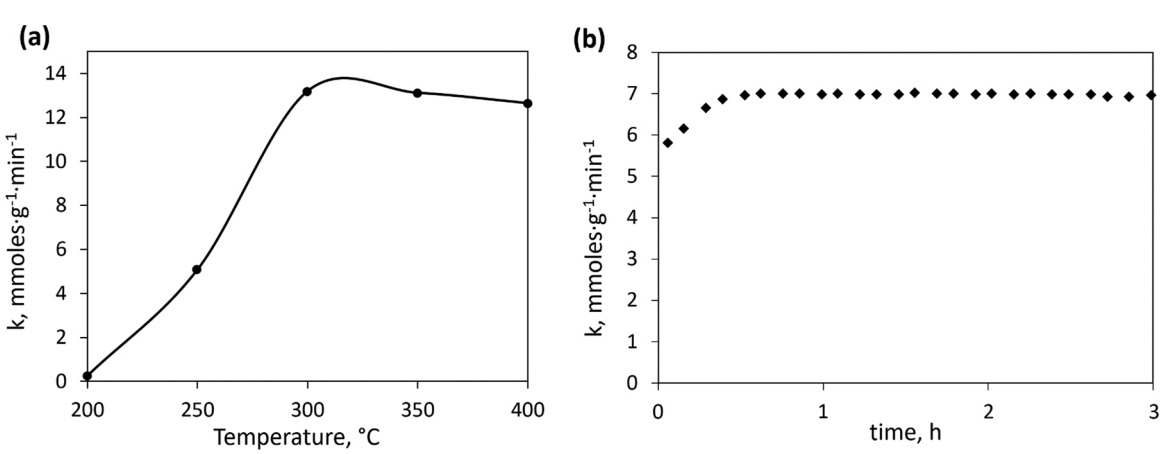

Fig. 5. (a) Temperature dependence of the Ni/CeO_2 catalytic activity in dark conditions; (b) Stability test of the Ni/CeO_2 catalyst.

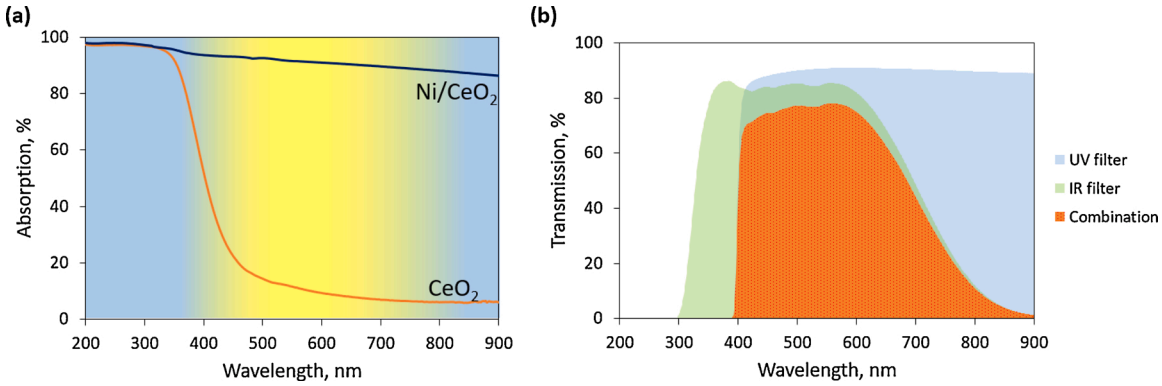

Fig. 6. (a) Reflectance absorption spectra of the bare CeO_2 and Ni/CeO_2 samples. Backround yellow color represents the visible irradiation band used in this work. (b) Transmission spectra of the bandpass filters used in this work. (For interpretation of the references to colour in this figure legend, the reader is referred to the web version of this article).

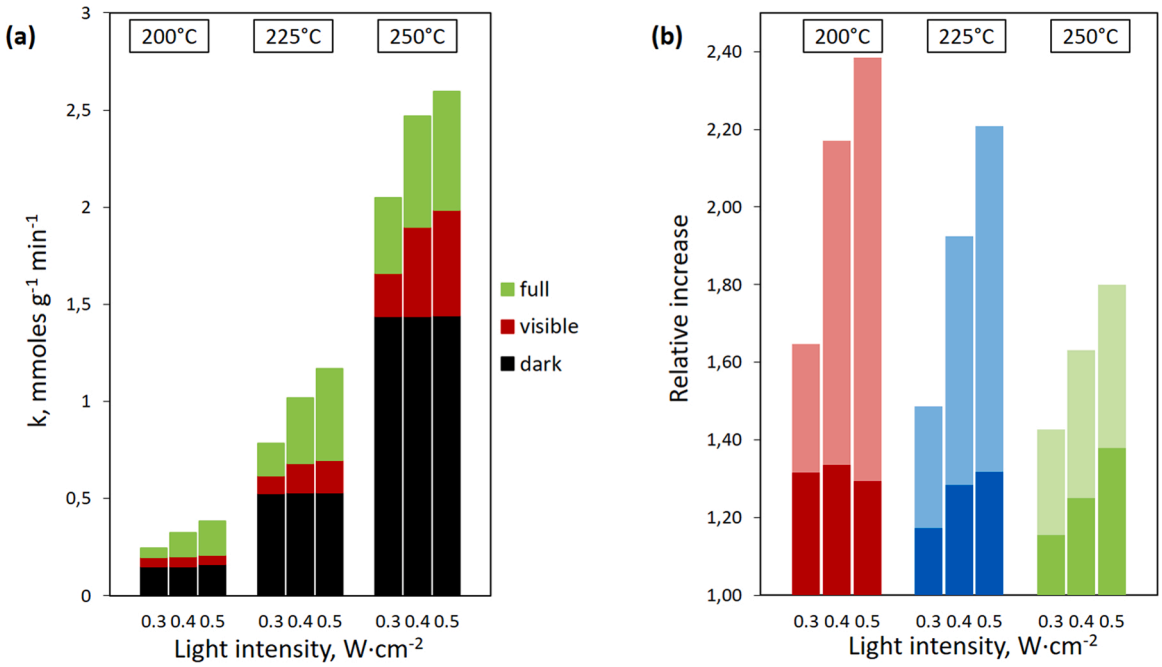

Fig. 7. Catalytic activity of the Ni/CeO_2 catalyst under visible light and full solar illumination of 3 to 5 suns at three different starting temperature points (200 °C, 225 °C and 250 °C) (a); Relative increase of the catalytic activity under illumination with respect to the dark reaction at the corresponding conditions (b). Solid bars correspond to the visible illumination, whereas the full bar corresponds to the full solar illumination. The light intensities correspond to the ones measured before introducing of the filters.

illumination is appearance of the carbonyl species on the Ni surface, identified at 2041 cm^{-1} (monocarbonyl), 1927 cm^{-1} (bridged carbonyl) and 1830 cm^{-1} (two-fold bridged carbonyl). These bands are growing with temperature increase up to 200 °C and afterwards turn to decrease along with formation of methane. This evidently indicates that carbonyls take part in the process of CO_2 hydrogenation to methane. The formation of carbonyls on the Ni surface may occur either through the direct dissociation of CO_2 or through decomposition of formate species.

3.5. Mechanism of photothermal CO_2 methanation

Typically, CO_2 hydrogenation on the Ni-based catalysts with inactive support, such as Al_2O_3 or SiO_2 occurs through the dissociation mechanism, i.e. formation of carbonyl or formate intermediates on the Ni^0 active sites [43]. On the other hand, Ni/CeO_2 catalysts were found to favor the associative mechanism of CO_2 methanation [59–61]. It means that the CO_2 molecules are chemisorbed as monodentate or bidentate carbonates on the reduced active sites of CeO_2, mostly present at the Ni/CeO_2 interface. At the same time, H_2 molecules dissociate on the metallic Ni clusters, facilitate C═O double-bond breaking and creation of the formates followed by their step-by-step hydrogenation to CH_4. This mechanism of CO_2 activation is energetically more favorable than the route through CO formation, and is ensured by high mobility of the oxygen vacancies in ceria. The latter allows partial reduction of the CeO_2 material by H_2 at the Ni/CeO_2 interface with subsequent formation of water molecules, while keeping the active sites reduced.

In dark conditions, the DRIFTS data recorded from our samples are in agreement with described above associative mechanism, indicating that stable bridged formate species serve as a main precursor for CO_2 hydrogenation to methane, probably through formation of formaldehyde and methoxy adsorbates. However, when the samples are illuminated, we observe immediate changes in the DRIFTS spectra. In particular, variations of the peaks suggest that hydrogen carbonates are more likely transformed to formates. Besides, we detect the appearance of carbonyl

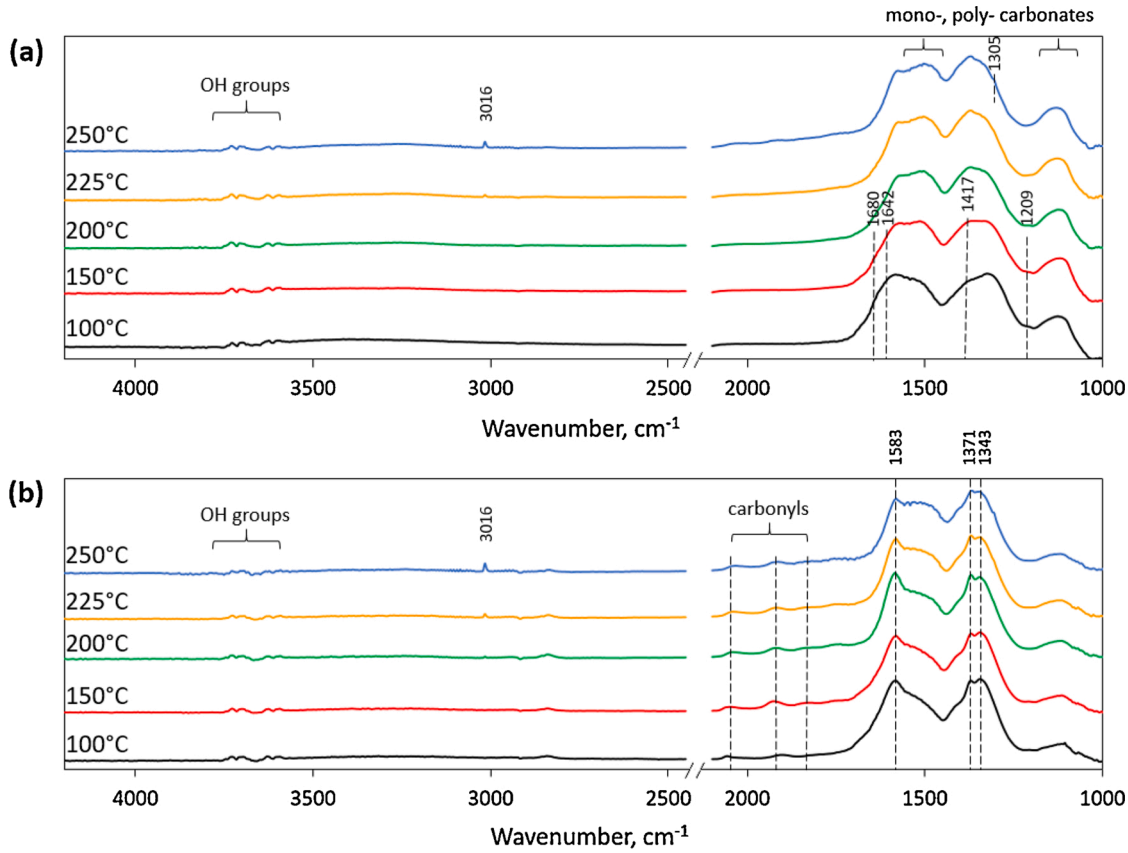

Fig. 8. In-situ DRIFTS spectra measured during CO_2 methanation over the Ni/CeO_2 catalyst (a) in dark conditions; (b) under solar illumination (5 suns).

species, which may be formed through dissociation of excessive formates [62].

Based on the obtained results, we suggest that illumination has a two-fold effect on the operational performance of the Ni/CeO_2 catalyst. First, visible and IR irradiations excite LSPR in Ni nanoparticles. Although plasmons in Ni are effectively damped, they result in strong local heating of the nickel nanoclusters with following heat dissipation to the surrounding oxide matrix. Such a plasmon-induced increase of the temperature facilitates the principal reaction channel at the Ni/CeO_2 interface.

On the other hand, the illumination is changing the surface chemistry of the catalyst as a result of photoelectronic processes. The obtained changes in the DRIFTS spectra indicate that illumination is promoting the stabilization of formate species from less stable hydrogen carbonates.

As the illumination of the catalyst is followed by the temperature increase (summarized in the Table S1), we have further analyzed the data from Fig. 7 in order to find out the nature of the improved catalytic activity. A thermally activated methanation reaction follows an exponential trend, i.e. $k \sim e^{-\frac{E_a}{kT}}$, where E_a is the activation energy of the reaction, or the rate-limiting step [63]. Therefore, $\ln(k) \sim -\frac{1}{T}$ for the

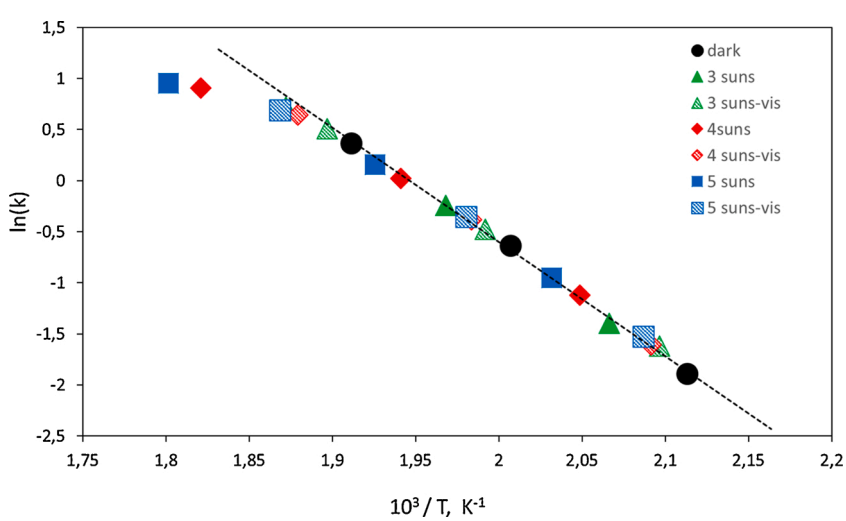

Fig. 9. Arrhenius slope of the temperature activated methanation reaction. The y axis indicates the natural logarithm of catalytic activity under different reaction conditions.

process that is fully controlled by the temperature. We have plotted a natural logarithm of the measured catalytic activities in all of the applied conditions versus the inverse temperature (Fig. 9). Remarkably, all the light-assisted measurements of the catalytic activity at low conversion rates were followed the same linear trend, indicating that the solar light illumination of the Ni/CeO_2 catalyst caused an increase of the catalytic activity due to the local temperature changes induced by plasmonic heating of the Ni nanoparticles.

From the Fig. 9 we have evaluated the Arrhenius slope for the methanation reaction (dashed line), with the activation energy of 0.96 eV. As discussed above, we attribute this energy to the methanation pathway that takes place through hydrogenation of the formates on ceria, presumably to the dissociation of formalin to formaldehyde, as it was shown in [64]. The light-induced increase in the concentration of formates, seen from the DRIFTS data, does not affect the main reaction channel, the latter being totally controlled by temperature. However, we have found that with increase of the illumination intensity the formate and carbonyl peaks on the DRIFTS spectra become more pronounced. We applied Gaussian multi-peak fitting to the spectra measured under dark conditions, 3 and 5 suns illumination in order to quantify the contribution of the formate intermediates depending on the intensity of the photon flux (Fig. S4). We found that the amount of adsorbed species is proportional to the power of the applied illumination, which indicates that the electronic effect of the solar illumination can be much more noticeable when higher light intensities are applied.

However, when reaching higher temperatures, one can observe a strong deviation from the linear trend towards lower catalytic activities, which points out on a new rate-limiting process that occurs at higher temperatures. As the selectivity to methane was not altered upon the temperature increase (see Table S2), this deviation cannot be explained by the activation of a side reaction, i.e. producing of carbon monoxide (reverse water gas-shift reaction), which is enabled at higher temperatures [65]. It is well known that the main deactivation pathways for the Ni-based catalysts are sintering of the Ni nanoparticles and coke formation [66]. However, these processes are also taking place at higher operation temperatures. On the other hand, Cárdenas-Arenas et al. conducted isotopic experiments on Ni/CeO_2 catalyst and showed that water desorption is the slowest step of the methanation mechanism [61]. As it was mentioned before, the light-assisted reaction was held in a custom-designed planar-type reactor under low gas flows. Apparently, at higher CO_2 conversion values the physisorbed water molecules, formed in big amounts during the reaction, are not efficiently removed from the reactor and block the active sites of the catalyst. Thus, in our case, desorption of water becomes a new rate-limiting step in the methanation process at high conversion rates. We assume that changing of the reactor design to being suitable for high-flow operation conditions will allow to examine the effect of strong illumination on methanation reaction rate with no limitations due to poisoning of the active sites by water molecules.

To understand the effect of different wavelengths on the catalyst we performed a series of DRIFTS experiments under solar illumination with different optical filters. The dark spectra were subtracted from the ones recorded under illumination in order to obtain differential data (Fig. 10). The results show that the UV part of the solar spectrum has the largest effect on the growth of formate and carbonyl peaks, while the visible light has a much weaker influence on the formate concentration. In the table S3 we have summarized the relative amounts of incident light intensities, used in this work. The intensity of transmitted light with the energy sufficient to excite band-to-band transitions in CeO_2 (250−400 nm) sums up to 10.5 % of the total solar spectrum, which results in a non-negligible amount of photogenerated carriers in the ceria support.

It should be noted that the real temperature of the illuminated catalyst is higher than the nominal value of the starting point. To ensure that the DRIFTS changes do not occur due to temperature-induced effects, caused by the heating of the catalyst under solar light, we have

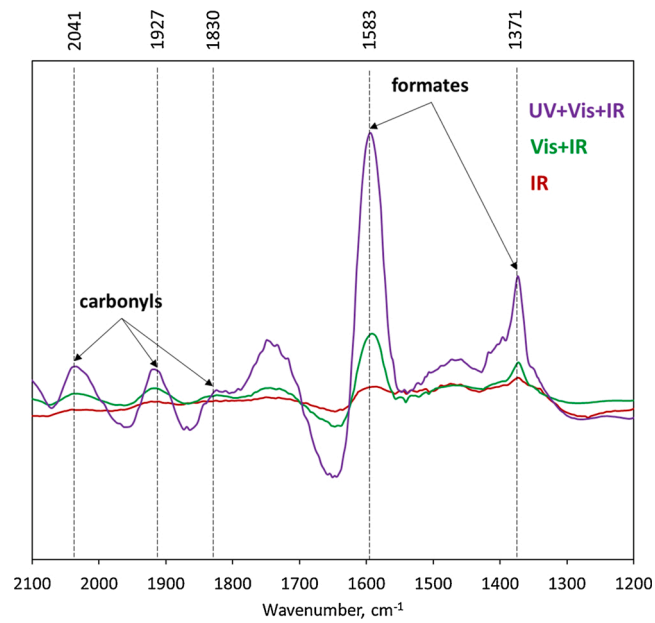

Fig. 10. Differential DRIFTS spectra of the Ni/CeO_2 catalyst measured at starting temperature of 200 °C under different wavelength illumination.

compared DRIFTS spectra of the catalyst under illumination with spectra recorded at elevated temperature in dark conditions (Fig. S5). The differential graph exhibits the same features as in the Fig. 10, which proves the non-thermal nature of the light-induced changes on the catalyst surface.

According to DRIFTS data, solar light promotes stabilization of the formate species on ceria surface. The increased concentration of formates, however, does not facilitate the overall methane production at the Ni/CeO_2 interface, which follows the Arrhenius slope (Fig. 9).

The surface of cerium oxide is known to be enriched with oxygen vacancies, which can trap photogenerated electrons under UV light excitation [67,68]. Furthermore, it was reported that chemisorption of CO_2 becomes favorable on the reduced CeO_2 surface with abundance of additional charge [57,69]. Therefore, it is plausible that UV and blue light illumination, present in the solar spectrum, can generate electron-hole pairs in ceria that activate surface vacancy sites and enhance sorption processes at CeO_2 surface. Photogenerated carriers facilitate transformation of the carbonate species to the more energetically stable formates, which is reflected in the corresponding changes of DRIFTS spectra. The concentration of formates is increased throughout the ceria support, including the sites apart from the Ni/CeO_2 interface. On the other hand, hydrogenation of formates, being the rate-limiting step of the methanation reaction, requires active hydrogen atoms, which are abundant at the interface with nickel nanoparticles. Thus, the formates adsorbed on ceria surface apart from the interface are lacking hydrogens and do not contribute effectively to the overall methane production.

The suggested mechanism of CO_2 methanation on the Ni/CeO_2 catalyst is schematically shown on Fig. 11 and can be described as follows. In dark conditions, CO_2 is adsorbed on the active sites at Ni/CeO_2 interface as bridged carbonates or hydrogen carbonates, which are further transformed to formates and monodentate carbonates. Under constant supply of hydrogen atoms from Ni nanoclusters, the formates at the interface are hydrogenated to methane. Solar illumination has a two-fold effect on the reaction. First, Ni nanoparticles exhibit a rapid local heating due to the strongly damped localized surface plasmons generated on Ni. This leads to an increase of the average temperature of the catalyst and to the overall increase of the methane production. Secondly, UV and visible illumination is enhancing photocatalytic properties of ceria. Photoinduced charge carriers facilitate transformation of

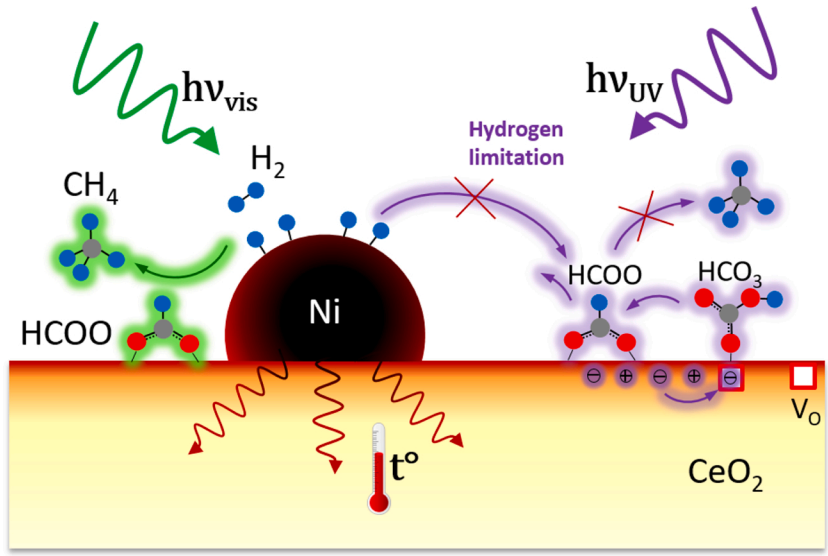

Fig. 11. Proposed mechanism of CO_2 methanation under solar illumination.

hydrogen carbonates to formates, giving rise to the corresponding peak on the DRIFTS spectra. However, the newly formed species adsorbed apart from the Ni/CeO_2 interface do not contribute to the methanation due to the limited hydrogen supply.

3.6. Energy consumption

One of the effective ways of exploiting the plasmon-induced photothermal effect of the Ni/CeO_2 catalyst for CO_2 methanation is to maintain the constant temperature of the reaction, by controlling the power supplied to the reactor. After compensation of the increased temperature to the initial value by reducing the power consumption, no improvement in the reaction rate was observed, which confirms that the photothermal effect of the illumination on the main reaction pathway is dominant at low temperatures and light intensities. However, we have measured the power, supplied to the heater of the reactor in the dark conditions (P_{dark}), and the corresponding power under illumination (P_{light}), reduced in order to maintain the working temperature at its initial value. Then, the reduced power consumption (RPC) for all of the experimental conditions used in this work was calculated according to the following formula:

$$RPC = \frac{P_{dark} - P_{light}}{P_{dark}} \cdot 100\%$$

The results are presented in the Fig. 12.

We can see that using concentrated sun illumination we are able to save up to 20 % of power applied for the conventional thermocatalytical approach to CO_2 methanation. Utilization of renewable solar energy source and an earth-abundant material with plasmonic properties for facilitation of effective thermal-driven CO_2 methanation allowed us to gain energy for further lowering of the cost, scalability and industrialization of the process.

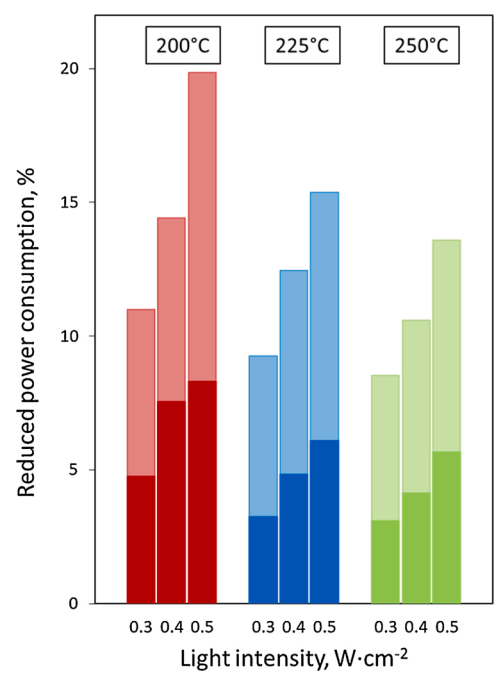

Fig. 12. Power consumption savings under visible light and full solar illumination of 3 to 5 suns at three different temperatures: 200 °C, 225 °C and 250 °C. Solid bars correspond to the visible illumination, whereas the full bar corresponds to the full solar illumination.

4. Conclusions

In summary, we have demonstrated that the catalytic activity of the methanation reaction can be improved by the photothermal effect due to localized surface plasmonic properties of the Ni nanoparticles in the Ni/CeO_2 catalyst under visible and infrared light illumination. Using of the mesoporous SBA-15 silica template allowed us to synthetize large-surface-area Ni/CeO_2 catalyst, which ensures highly stable and efficient conversion of CO_2 (80 %) with high selectivity to methane (95 %). The obtained catalyst exhibits up to a 2.4-fold increase in the reaction rate under solar light illumination, which allowed us to decrease the power consumption by 20 % with respect to the dark conditions.

In-situ DRIFTS analysis revealed the mechanism of the CO_2 methanation in dark and light-assisted conditions. In dark conditions the CO_2 methanation is following the associative route through formate hydrogenation on CeO_2, using Ni^0 active sites only for H_2 dissociation and spillover. When illuminating the catalyst with solar light, two main effects were observed. On the one hand, the visible and IR illumination results in a strong photothermal plasmon-induced effect, followed by local heating and enhanced methane production. On the other hand, UV and blue light induced photogenerated free carriers in CeO_2 can improve the CO_2 coordination and promote the creation of formates. However, their further hydrogenation remains fully controlled by the

photothermally activated process due to the limited hydrogen supply to the formate species. Investigation of the rate-limiting step by means of the first-principles calculations will be the subject of the future work.

At high conversion rates, the activity of the Ni/CeO_2 catalyst in the current reactor design is damped by the slow water desorption process from the active Ni^0 sites. Therefore, we have utilized the plasmon-induced photothermal effect of the Ni/CeO_2 catalyst for CO_2 methanation by operating at low reaction temperatures, reducing the power supplied to the reactor. Nevertheless, we believe that new reactor design may open a possibility of a thorough study and exploitation of the new light-induced methanation route at higher illumination intensities and conversion rates, thus further reducing the power consumed by the reactor.

Our results emphasize the two-fold effect of solar illumination on the plasmonic Ni-based catalysts: photothermal and electronic. Hence, we expect the combined photo- and thermocatalytical approach to provide a promising pathway for Ni-based heterogeneous catalysts for green CO_2 hydrogenation.

CRediT authorship contribution statement

Viktoria Golovanova: Writing - original draft, Conceptualization, Investigation. **Maria Chiara Spadaro:** Investigation, Writing - review & editing. **Jordi Arbiol:** Investigation, Writing - review & editing. **Viacheslav Golovanov:** Writing - review & editing, Conceptualization. **Tapio T. Rantala:** Writing - review & editing. **Teresa Andreu:** Writing - review & editing, Supervision, Conceptualization. **Joan Ramón Morante:** Writing - review & editing, Supervision, Conceptualization.

Declaration of Competing Interest

The authors declare that they have no known competing financial interests or personal relationships that could have appeared to influence the work reported in this paper.

Acknowledgments

This work has been done in the framework of the doctorate programme in Materials Science of the Autonomous University of Barcelona. V. Golovanova has received funding from the European Union's Horizon 2020 research and innovation programme under the Marie Skłodowska-Curie grant agreement No 754397. Authors acknowledge Generalitat de Catalunya for financial support through the CERCA Programme, M2E (2017 SGR 1246) and the CSC – IT Center for Science, Espoo, Finland for provided resources. IREC also acknowledges additional support by the European Regional Development Funds (ERDF, FEDER) and by MINECO coordinated projects MAT2014-59961-C2, ENE2016-80788-C5-5-R and ENE2017-85087-C3.

M. C. Spadaro and J. Arbiol acknowledge funding from Generalitat de Catalunya 2017 SGR 327. ICN2 is supported by the Severo Ochoa programme from Spanish MINECO (Grant No. SEV-2017-0706) and is funded by the CERCA Programme / Generalitat de Catalunya. M. C. Spadaro has received funding from the European Union's Horizon 2020 research and innovation programme under the Marie Skłodowska-Curie grant agreement No. 754510 (PROBIST) and the Severo Ochoa programme.

Appendix A. Supplementary data

Supplementary material related to this article can be found, in the online version, at doi:https://doi.org/10.1016/j.apcatb.2021.120038.

References

[1] D.R. Lide, CRC Handbook of Chemistry and Physics, 88th ed., Taylor Fr., 2007 https://doi.org/10.1021/ja077011d.

[2] G. Centi, E.A. Quadrelli, S. Perathoner, Catalysis for CO_2 conversion: a key technology for rapid introduction of renewable energy in the value chain of chemical industries, Energy Environ. Sci. 6 (2013) 1711–1731, https://doi.org/10.1039/c3ee00056g.

[3] A. Álvarez, M. Borges, J.J. Corral-Pérez, J.G. Olcina, L. Hu, D. Cornu, R. Huang, D. Stoian, A. Urakawa, CO_2 activation over catalytic surfaces, Chem. Phys. Chem. 18 (22) (2017) 3135–3141, https://doi.org/10.1002/cphc.201700782.

[4] M. Younas, L. Loong Kong, M.J.K. Bashir, H. Nadeem, A. Shehzad, S. Sethupathi, Recent advancements, fundamental challenges, and opportunities in catalytic methanation of CO_2, Energy Fuels 30 (11) (2016) 8815–8831, https://doi.org/10.1021/acs.energyfuels.6b01723.

[5] M.A.A. Aziz, A.A. Jalil, S. Triwahyono, A. Ahmad, CO2 methanation over heterogeneous catalysts: recent progress and future prospects, Green Chem. 17 (2015) 2647–2663, https://doi.org/10.1039/c5gc00119f.

[6] J. Wu, Y. Huang, W. Ye, Y. Li, CO_2 reduction: from the electrochemical to photochemical approach, Adv. Sci. 14 (11) (2017) 1700194, https://doi.org/10.1002/advs.201700194.

[7] R.P. Ye, J. Ding, W. Gong, M.D. Argyle, Q. Zhong, Y. Wang, C.K. Russell, Z. Xu, A. G. Russell, Q. Li, M. Fan, Y.G. Yao, CO_2 hydrogenation to high-value products via heterogeneous catalysis, Nat. Commun. 10 (2019) 5698, https://doi.org/10.1038/s41467-019-13638-9.

[8] K. Manthiram, B.J. Beberwyck, A.P. Alivisatos, Enhanced electrochemical methanation of carbon dioxide with a dispersible nanoscale copper catalyst, J. Am. Chem. Soc. 136 (38) (2014) 13319–13325, https://doi.org/10.1021/ja5065284.

[9] M.C. Bacariza, M. Biset-Peiró, I. Graça, J. Guilera, J. Morante, J.M. Lopes, T. Andreu, C. Henriques, DBD plasma-assisted CO_2 methanation using zeolite-based catalysts: Structure composition-reactivity approach and effect of Ce as promoter, J. CO_2 Util. 26 (2018) 202–211, https://doi.org/10.1016/j.jcou.2018.05.013.

[10] Y. Ge, T. He, D. Han, G. Li, R. Zhao, J. Wu, Plasma-assisted CO_2 methanation: effects on the low-temperature activity of an Ni–Ce catalyst and reaction performance, R. Soc. Open Sci. 6 (2020), 190750, https://doi.org/10.1098/rsos.190750.

[11] X. Dai, Y. Sun, Reduction of carbon dioxide on photoexcited nanoparticles of VIII group metals, Nanoscale 11 (2019) 16723–16732, https://doi.org/10.1039/c9nr05971g.

[12] U. Ulmer, T. Dingle, P.N. Duchesne, R.H. Morris, A. Tavasoli, T. Wood, G.A. Ozin, Fundamentals and applications of photocatalytic CO_2 methanation, Nat. Commun. 10 (2019) 3169, https://doi.org/10.1038/s41467-019-10996-2.

[13] P.G. O'Brien, A. Sandhel, T.E. Wood, A.A. Jelle, L.B. Hoch, D.D. Perovic, C. A. Mims, G.A. Ozin, Photomethanation of gaseous CO_2 over Ru/silicon nanowire catalysts with visible and near-infrared photons, Adv. Sci. 1 (1) (2014) 1400001, https://doi.org/10.1002/advs.201400001.

[14] Ş. Neaţu, J.A. Maciá-Agulló, P. Concepciòn, H. Garcia, Gold-copper nanoalloys supported on TiO_2 as photocatalysts for CO_2 reduction by water, J. Am. Chem. Soc. 136 (45) (2014) 15969–15976, https://doi.org/10.1021/ja506433k.

[15] F. Sastre, A.V. Puga, L. Liu, A. Corma, H. García, Complete photocatalytic reduction of CO_2 to methane by H_2 under solar light irradiation, J. Am. Chem. Soc. 136 (19) (2014) 6798–6801, https://doi.org/10.1021/ja500924t.

[16] W.N. Wang, W.J. An, B. Ramalingam, S. Mukherjee, D.M. Niedzwiedzki, S. Gangopadhyay, P. Biswas, Size and structure matter: enhanced CO_2 photoreduction efficiency by size-resolved ultrafine Pt nanoparticles on TiO_2 single crystals, J. Am. Chem. Soc. 134 (27) (2012) 11276–11281, https://doi.org/10.1021/ja304075b.

[17] O. Ola, M. Mercedes Maroto-Valer, Role of catalyst carriers in CO_2 photoreduction over nanocrystalline nickel loaded TiO_2-based photocatalysts, J. Catal. 309 (2014) 300–308, https://doi.org/10.1016/j.jcat.2013.10.016.

[18] S.C. Warren, E. Thimsen, Plasmonic solar water splitting, Energy Environ. Sci. 5 (1) (2012) 5133–5146, https://doi.org/10.1039/c1ee02875h.

[19] P. Wang, B. Huang, Y. Dai, M.H. Whangbo, Plasmonic photocatalysts: harvesting visible light with noble metal nanoparticles, Phys. Chem. Chem. Phys. 14 (2012) 9813–9825, https://doi.org/10.1039/c2cp40823f.

[20] H. Song, X. Meng, T.D. Dao, W. Zhou, H. Liu, L. Shi, H. Zhang, T. Nagao, T. Kako, J. Ye, Light-enhanced carbon dioxide activation and conversion by effective plasmonic coupling effect of Pt and Au nanoparticles, ACS Appl. Mater. Interfaces 10 (1) (2018) 408–416, https://doi.org/10.1021/acsami.7b13043.

[21] H.M. Gong, L. Zhou, X.R. Su, S. Xiao, S.D. Liu, Q.Q. Wang, Illuminating dark plasmons of silver nanoantenna rings to enhance exciton-plasmon interactions, Adv. Funct. Mater. 19 (2) (2009) 298–303, https://doi.org/10.1002/adfm.200801151.

[22] G. Kumari, X. Zhang, D. Devasia, J. Heo, P.K. Jain, Watching visible light-driven CO_2 reduction on a plasmonic nanoparticle catalyst, ACS Nano 12 (8) (2018) 8330–8340, https://doi.org/10.1021/acsnano.8b03617.

[23] W. Hou, W.H. Hung, P. Pavaskar, A. Goeppert, M. Aykol, S.B. Cronin, Photocatalytic conversion of CO_2 to hydrocarbon fuels via plasmon-enhanced absorption and metallic interband transitions, ACS Catal. 1 (8) (2011) 929–936, https://doi.org/10.1021/cs2001434.

[24] C.G. Silva, R. Juá rez, T. Marino, R. Molinari, H. García, Influence of excitation wavelength (UV or visible light) on the photocatalytic activity of titania containing gold nanoparticles for the generation of hydrogen or oxygen from water, J. Am. Chem. Soc. 133 (3) (2011) 595–602, https://doi.org/10.1021/ja1086358.

[25] H. Liu, X. Meng, T.D. Dao, L. Liu, P. Li, G. Zhao, T. Nagao, L. Yang, J. Ye, Light assisted CO_2 reduction with methane over SiO_2 encapsulated Ni nanocatalysts for boosted activity and stability, J. Mater. Chem. A 5 (21) (2017) 10567–10573, https://doi.org/10.1039/c7ta00704c.

[26] X. Meng, T. Wang, L. Liu, S. Ouyang, P. Li, H. Hu, T. Kako, H. Iwai, A. Tanaka, J. Ye, Photothermal Conversion of CO_2 into CH_4 with H_2 over Group VIII Nanocatalysts: An Alternative Approach for Solar Fuel Production, Angew. Chem. 126 (43) (2014) 11662–11666, https://doi.org/10.1002/ange.201404953.

[27] A.M. Watson, X. Zhang, R. Alcaraz De La Osa, J.M. Sanz, F. González, F. Moreno, G. Finkelstein, J. Liu, H.O. Everitt, Rhodium nanoparticles for ultraviolet plasmonics, Nano Lett. 15 (2) (2015) 1095–1100, https://doi.org/10.1021/nl5040623.

[28] A. Picciotto, G. Pucker, L. Torrisi, P. Bellutti, F. Caridi, A. Bagolini, Evidence of plasmon resonances of nickel particles deposited by pulsed laser ablation, Radiat. Eff. Defects Solids 163 (4) (2008) 513–518, https://doi.org/10.1080/10420150701780656.

[29] Z. Xiong, X. Chen, X. Wang, L. Peng, D. Yan, H. Lei, Y. Fu, J. Wu, Z. Li, X. An, W. Wu, Size dependence of plasmon absorption of Ni nanoparticles embedded in $BaTiO_3$ /$SrTiO_3$ superlattices, Appl. Surf. Sci. 268 (2013) 524–528, https://doi.org/10.1016/j.apsusc.2012.12.161.

[30] A. Alarcón, J. Guilera, J.A. Díaz, T. Andreu, Optimization of nickel and ceria catalyst content for synthetic natural gas production through CO_2 methanation, Fuel Process. Technol. 193 (2019) 114–122, https://doi.org/10.1016/j.fuproc.2019.05.008.

[31] K. Wu, J. Chen, J.R. McBride, T. Lian, Efficient hot-electron transfer by a plasmon-induced interfacial charge-transfer transition, Science 349 (6248) (2015) 632–635, https://doi.org/10.1126/science.aac5443.

[32] S. Tan, A. Argondizzo, J. Ren, L. Liu, J. Zhao, H. Petek, Plasmonic coupling at a metal/semiconductor interface, Nat. Photonics 11 (2017) 806–812, https://doi.org/10.1038/s41566-017-0049-4.

[33] L. Mascaretti, A. Naldoni, Hot electron and thermal effects in plasmonic photocatalysis, J. Appl. Phys. 128 (2020) 041101, https://doi.org/10.1063/5.0013945.

[34] S. He, J. Huang, J.L. Goodsell, A. Angerhofer, W.D. Wei, Plasmonic nickel–TiO_2 heterostructures for visible-light-driven photochemical reactions, Angew. Chem. Int. Ed. 58 (18) (2019) 6038–6041, https://doi.org/10.1002/anie.201901987.

[35] X. Zhang, X. Li, D. Zhang, N.Q. Su, W. Yang, H.O. Everitt, J. Liu, Product selectivity in plasmonic photocatalysis for carbon dioxide hydrogenation, Nat. Commun. 8 (2017), 14542, https://doi.org/10.1038/ncomms14542.

[36] C. Kim, S. Hyeon, J. Lee, W.D. Kim, D.C. Lee, J. Kim, H. Lee, Energy-efficient CO_2 hydrogenation with fast response using photoexcitation of CO_2 adsorbed on metal catalysts, Nat. Commun. 9 (2018), 3027, https://doi.org/10.1038/s41467-018-05542-5.

[37] J.S. Pelli Cresi, M.C. Spadaro, S. D'Addato, S. Valeri, S. Benedetti, A. Di Bona, D. Catone, L. Di Mario, P. O'Keeffe, A. Paladini, G. Bertoni, P. Luches, Highly efficient plasmon-mediated electron injection into cerium oxide from embedded silver nanoparticles, Nanoscale 11 (21) (2019) 10282–10291, https://doi.org/10.1039/c9nr01390c.

[38] J. Chen, Y. Zhou, R. Li, X. Wang, G.Z. Chen, Highly-dispersed nickel nanoparticles decorated titanium dioxide nanotube array for enhanced solar light absorption, Appl. Surf. Sci. 464 (2019) 716–724, https://doi.org/10.1016/j.apsusc.2018.09.091.

[39] Q. Zhang, M. Mao, Y. Li, Y. Yang, H. Huang, Z. Jiang, Q. Hu, S. Wu, X. Zhao, Novel photoactivation promoted light-driven CO_2 reduction by CH_4 on Ni/CeO_2 nanocomposite with high light-to-fuel efficiency and enhanced stability, Appl. Catal. B Environ. 239 (30) (2018) 555–564, https://doi.org/10.1016/j.apcatb.2018.08.052.

[40] J. Albero, H. Garcia, A. Corma, Temperature dependence of solar light assisted CO_2 reduction on Ni based photocatalyst, Top. Catal. 59 (2016) 787–791, https://doi.org/10.1007/s11244-016-0550-x.

[41] E. Rossinyol, J. Arbiol, F. Peiró, A. Cornet, J.R. Morante, B. Tian, T. Bo, D. Zhao, Nanostructured metal oxides synthesized by hard template method for gas sensing applications, Sens. Actuators B Chem. 109 (1) (2005) 57–63, https://doi.org/10.1016/j.snb.2005.03.016.

[42] L. Almar, T. Andreu, A. Morata, M. Torrell, L. Yedra, S. Estradé, F. Peiró, A. Tarancón, High-surface-area ordered mesoporous oxides for continuous operation in high temperature energy applications, J. Mater. Chem. A 2 (2014) 3134–3141, https://doi.org/10.1039/c3ta13951d.

[43] B. Miao, S.S.K. Ma, X. Wang, H. Su, S.H. Chan, Catalysis mechanisms of CO_2 and CO methanation, Catal. Sci. Technol. 6 (2016) 4048–4058, https://doi.org/10.1039/c6cy00478d.

[44] V. La Parola, G. Pantaleo, A. Venezia, Effects of synthesis on the structural properties and methane partial oxidation activity of Ni/CeO_2 catalyst, Catalysts 8 (5) (2018) 220, https://doi.org/10.3390/catal8050220.

[45] S. Xu, X. Wang, Highly active and coking resistant Ni/CeO_2-ZrO_2 catalyst for partial oxidation of methane, Fuel 84 (5) (2005) 563–567, https://doi.org/10.1016/j.fuel.2004.10.008.

[46] D. Chen, H. Hao, J. Yu, J. Liu, J. Lu, F. Liu, G. Wan, S. He, Y. Luo, Structural/surface characterization and catalytic evaluation of rare-earth (Y, Sm and La) doped ceria composite oxides for CH_3SH catalytic decomposition, Appl. Surf. Sci. 390 (2016) 959–967, https://doi.org/10.1016/j.apsusc.2016.08.129.

[47] R. Murugan, G. Vijayaprasath, T. Mahalingam, G. Ravi, Enhancement of room temperature ferromagnetic behavior of rf sputtered Ni-CeO_2 thin films, Appl. Surf. Sci. 390 (2016) 583–590, https://doi.org/10.1016/j.apsusc.2016.08.166.

[48] M.J. Hÿtch, E. Snoeck, R. Kilaas, Quantitative measurement of displacement and strain fields from HREM micrographs, Ultramicroscopy 74 (3) (1998) 131–146, https://doi.org/10.1016/S0304-3991(98)00035-7.

[49] S. Tada, T. Shimizu, H. Kameyama, T. Haneda, R. Kikuchi, Ni/CeO_2 catalysts with high CO_2 methanation activity and high CH_4 selectivity at low temperatures, Int. J. Hydrogen Energy 37 (7) (2012) 5527–5531, https://doi.org/10.1016/j.ijhydene.2011.12.122.

[50] G. Zhou, H. Liu, K. Cui, A. Jia, G. Hu, Z. Jiao, Y. Liu, X. Zhang, Role of surface Ni and Ce species of Ni/CeO_2 catalyst in CO_2 methanation, Appl. Surf. Sci. 383 (2016) 248–252, https://doi.org/10.1016/j.apsusc.2016.04.180.

[51] S. Soni, S. Kumar, B. Dalela, S. Kumar, P.A. Alvi, S. Dalela, Defects and oxygen vacancies tailored structural and optical properties in CeO_2 nanoparticles doped with Sm^{3+} cation, J. Alloys Compd. 752 (2018) 520–531, https://doi.org/10.1016/j.jallcom.2018.04.157.

[52] H. Liu, T.D. Dao, L. Liu, X. Meng, T. Nagao, J. Ye, Light assisted CO 2 reduction with methane over group VIII metals: universality of metal localized surface plasmon resonance in reactant activation, Appl. Catal. B Environ. 209 (2017) 183–189, https://doi.org/10.1016/j.apcatb.2017.02.080.

[53] Z. Xin, L. Lu, B. Wang, X. Wang, K. Zhu, Z. Xu, Z. Yu, S. Yan, Z. Zou, Lewis acid activated CO_2 reduction over a Ni modified Ni-Ge hydroxide driven by visible-infrared light, Dalton Trans. 48 (2019) 1672–1679, https://doi.org/10.1039/c8dt04408b.

[54] H. Liu, H. Song, X. Meng, L. Yang, J. Ye, Light irradiation enhanced CO_2 reduction with methane: a case study in size-dependent optical property of Ni nanoparticles, Catal. Today 335 (2019) 187–192, https://doi.org/10.1016/j.cattod.2018.11.005.

[55] G.E. Jonsson, V. Miljkovic, A. Dmitriev, Nanoplasmon-enabled macroscopic thermal management, Sci. Rep. 4 (2014), 5111, https://doi.org/10.1038/srep05111.

[56] N.M. Martin, F. Hemmingsson, A. Schaefer, M. Ek, L.R. Merte, U. Hejral, J. Gustafson, M. Skoglundh, A.C. Dippel, O. Gutowski, M. Bauer, P.A. Carlsson, Structure-function relationship for CO_2 methanation over ceria supported Rh and Ni catalysts under atmospheric pressure conditions, Catal. Sci. Technol. 9 (2019) 1644–1653, https://doi.org/10.1039/c8cy02097c.

[57] F. Wang, S. He, H. Chen, B. Wang, L. Zheng, M. Wei, D.G. Evans, X. Duan, Active site dependent reaction mechanism over Ru/CeO_2 catalyst toward CO_2 methanation, J. Am. Chem. Soc. 138 (19) (2016) 6298–6305, https://doi.org/10.1021/jacs.6b02762.

[58] Y. Yang, C.A. Mims, R.S. Disselkamp, J.H. Kwak, C.H.F. Peden, C.T. Campbell, (Non)formation of methanol by direct hydrogenation of formate on copper catalysts, J. Phys. Chem. C 114 (40) (2010) 17205–17211, https://doi.org/10.1021/jp104068k.

[59] P.A.U. Aldana, F. Ocampo, K. Kobl, B. Louis, F. Thibault-Starzyk, M. Daturi, P. Bazin, S. Thomas, A.C. Roger, Catalytic CO_2 valorization into CH_4 on Ni-based ceria-zirconia. Reaction mechanism by operando IR spectroscopy, Catal. Today 215 (2013) 201–207, https://doi.org/10.1016/j.cattod.2013.02.019.

[60] S.M. Lee, Y.H. Lee, D.H. Moon, J.Y. Ahn, D.D. Nguyen, S.W. Chang, S.S. Kim, Reaction mechanism and catalytic impact of Ni/CeO_{2-x} catalyst for low-temperature CO_2 methanation, Ind. Eng. Chem. Res. 58 (20) (2019) 8656–8662, https://doi.org/10.1021/acs.iecr.9b00983.

[61] A. Cárdenas-Arenas, A. Quindimil, A. Davó-Quiñonero, E. Bailón-García, D. Lozano-Castelló, U. De-La-Torre, B. Pereda-Ayo, J.A. González-Marcos, J. R. González-Velasco, A. Bueno-López, Isotopic and *in situ* DRIFTS study of the CO_2 methanation mechanism using Ni/CeO_2 and Ni/Al_2O_3 catalysts, Appl. Catal. B Environ. 265 (2020), 118538, https://doi.org/10.1016/j.apcatb.2019.118538.

[62] A. Westermann, B. Azambre, M.C. Bacariza, I. Graça, M.F. Ribeiro, J.M. Lopes, C. Henriques, The promoting effect of Ce in the CO_2 methanation performances on NiUSY zeolite: a FTIR *in situ/operando* study, Catal. Today 283 (2017) 74–81, https://doi.org/10.1016/j.cattod.2016.02.031.

[63] C.E. Verostko, R.K. Forsythe, A Study of the Sebatier-Methanation Reaction, 1974, https://doi.org/10.4271/740933.

[64] Z. Cheng, C.S. Lo, Mechanistic and microkinetic analysis of CO_2 hydrogenation on ceria, Phys. Chem. Chem. Phys. 18 (2016) 7987–7996, https://doi.org/10.1039/c5cp07469j.

[65] L. Pastor-Pérez, F. Baibars, E. Le Sache, H. Arellano-García, S. Gu, T.R. Reina, CO_2 valorisation via Reverse Water-Gas Shift reaction using advanced Cs doped Fe-Cu/Al_2O_3 catalysts, J. CO_2 Util. 21 (2017) 423–428, https://doi.org/10.1016/j.jcou.2017.08.009.

[66] S. Abelló, C. Berrueco, D. Montané, High-loaded nickel-alumina catalyst for direct CO_2 hydrogenation into synthetic natural gas (SNG), Fuel 113 (2013) 598–609, https://doi.org/10.1016/j.fuel.2013.06.012.

[67] B. Choudhury, P. Chetri, A. Choudhury, Oxygen defects and formation of Ce^{3+} affecting the photocatalytic performance of CeO_2 nanoparticles, RSC Adv. 4 (2014) 4663–4671, https://doi.org/10.1039/c3ra44603d.

[68] C. Yang, J. Yang, X. Duan, G. Hu, Q. Liu, S. Ren, J. Li, M. Kong, Roles of photo-generated holes and oxygen vacancies in enhancing photocatalytic performance over CeO_2 prepared by molten salt method, Adv. Powder Technol. 31 (9) (2020) 4072–4081, https://doi.org/10.1016/j.apt.2020.08.017.

[69] K.R. Hahn, M. Iannuzzi, A.P. Seitsonen, J. Hutter, Coverage effect of the CO_2 adsorption mechanisms on CeO_2(111) by first principles analysis, J. Phys. Chem. C 117 (4) (2013) 1701–1711, https://doi.org/10.1021/jp309565u.